

# CHORUS

This is the accepted manuscript made available via CHORUS. The article has been published as:

## Neutron scattering and $\mu$ SR investigations of quasi-one-dimensional magnetism in the spin = 3/2 compound $\text{Li}_3\text{RuO}_4$

P. Manuel, D. T. Adroja, Per-Anker Lindgard, A. D. Hillier, P. D. Battle, Won-Joon Son, and Myung-Hwan Whangbo

Phys. Rev. B **84**, 174430 — Published 21 November 2011

DOI: [10.1103/PhysRevB.84.174430](https://doi.org/10.1103/PhysRevB.84.174430)

**Neutron scattering and  $\mu$ SR investigations of quasi-one dimensional magnetism in the spin=3/2 compound:  $\text{Li}_3\text{RuO}_4$**

P. Manuel<sup>1\*</sup>, D.T. Adroja<sup>1\*</sup>, Per-Anker Lindgard<sup>2</sup>, A.D. Hillier<sup>1</sup>, P. D. Battle<sup>3</sup>, Won-Joon Son<sup>4</sup>  
and Myung-Hwan Whangbo<sup>4</sup>

<sup>1</sup>*ISIS Facility, Rutherford Appleton Laboratory, Chilton, Didcot, Oxon, OX11 0QX, U.K.*

<sup>2</sup>*Materials Research Division, Risø National Laboratory for Sustainable Energy, DTU, DK-4000 Roskilde Denmark*

<sup>3</sup>*Inorganic Chemistry Laboratory, Oxford University, South Parks Road, Oxford, OX1 3QR, U.K.*

<sup>4</sup>*Department of Chemistry, North Carolina State University, Raleigh, North Carolina 276958204, USA*

(Dated: 5<sup>th</sup> Oct. 2011)

**Abstract**

The  $S=3/2$ , quasi-1D zig-zag chain Heisenberg antiferromagnet  $\text{Li}_3\text{RuO}_4$  has been investigated using inelastic neutron scattering, neutron diffraction and  $\mu$ SR measurements on a powder sample. Our neutron diffraction and  $\mu$ SR studies confirm a long-range ordering of the magnetic moments on the  $\text{Ru}^{5+}$  cations below 40 K. The magnetic excitations were measured at various temperatures above and below the three-dimensional (3D) ordering temperature in order to understand the broad peak observed in the temperature dependence of the magnetic susceptibility. At 5 K we have observed two well-defined magnetic excitations at 5.5 meV and 8.5 meV, and a weak low-energy peak near  $\sim 2$  meV. We interpret the 5.5 meV energy peak as a 1D zone boundary mode and that at 8.5 meV as arising from a maximum away from the zone-boundary in the dispersion curve for spin-wave modes along the chain of  $\text{Ru}^{5+}$  ions. The weaker peak near 2 meV is thought to arise from a weak inter-chain coupling. Our data are best reproduced using a model with three intrachain interactions and one weak interchain interaction. The experimental spin-exchange interactions are in good agreement with those calculated for a 1D model by DFT methods. Furthermore, above  $T_N$  we observe strong diffuse scattering at the same Q-position as

the 5.5 meV mode, which suggests the presence of short-range magnetic correlations above  $T_N$ . We have estimated the correlation length,  $\xi \sim 2.9 \text{ \AA}$  at 50 K, which is close to 2.99  $\text{\AA}$ , the shortest distance between the  $\text{Ru}^{5+}$  cations along the zig-zag chain.

PACS No: 75.30.Ds, 78.70.Nx, 75.50.-y

Keywords: Spin-wave investigations, low-dimensional magnetism, Antiferromagnetic ordering,  $\text{Li}_3\text{RuO}_4$ ,  $\mu\text{SR}$ , Neutron diffraction.

\* E-mail address: [Devashibhai.adroja@stfc.ac.uk](mailto:Devashibhai.adroja@stfc.ac.uk); [Pascal.manuel@stfc.ac.uk](mailto:Pascal.manuel@stfc.ac.uk)

## 1. Introduction

In the past few decades,  $3d$  transition-metal oxide systems such as high-temperature superconducting cuprates, nickelates and colossal-magnetoresistive manganites have generated a great deal of interest in condensed-matter physics research due to the amazing variety of their ground-state properties, and, in particular the interplay between magnetism and (super)conductivity. Magnetism is much less common in  $4d$  transition-metal oxides than in  $3d$ -based oxides because both the on-site Stoner and Coulomb parameters are lower, whereas the bandwidths tend to be larger because the more extended nature of  $4d$  orbitals relative to their  $3d$  counterparts leads to stronger hybridization between the  $d$  orbitals and the oxygen  $2p$  orbitals. In fact, amongst the  $4d$ -oxide systems, only those containing ruthenium exhibit long-range ordered magnetism. Consequently, in recent years, there has been a considerable increase in the interest in ruthenium-based  $4d$  oxide systems, known as ruthenates. These adopt a variety of crystal structures, including perovskite, layered structures and the three dimensional (3D) geometrically-frustrated pyrochlore. Although still not as well studied as  $3d$ -based systems, many  $\text{Ru}^{4+}$  compounds have now been shown to exhibit very exciting physical properties including orbital ordering in  $\text{La}_4\text{Ru}_2\text{O}_{10}$  [1], possible Haldane gap formation in  $\text{Tl}_2\text{Ru}_2\text{O}_7$  [2], unconventional superconductivity in  $\text{Sr}_2\text{RuO}_4$  ( $T_C=1.5$  K) [3], non-Fermi liquid behaviour in  $\text{La}_4\text{Ru}_6\text{O}_{19}$  [4] and unusual ferromagnetic ordering in  $\text{SrRuO}_3$  ( $T_C=165$  K) [5]. Furthermore, resistivity and optical studies have shown non-Fermi-liquid behaviour in the paramagnetic state of both  $\text{SrRuO}_3$  and  $\text{CaRuO}_3$  [5]. It is noteworthy that even though  $\text{Tl}_2\text{Ru}_2\text{O}_7$  has a crystal structure without any low-dimensional characteristics, the magnetic interactions are mainly 1D, due to orbital ordering of the  $\text{Ru}^{4+}$  ions.

The observation of such a wide range of electronic properties suggests that ruthenates sit on the boundary between magnetic and non-magnetic ground states, and are thus relevant to the study of quantum magnetism. It is important to recognise that the chemistry of ruthenium is not restricted to  $\text{Ru}^{4+}$ . Mixed-metal oxides containing  $\text{Ru}^{5+}$  have also been synthesized and many of them have been shown to have an antiferromagnetic ground state, for example  $\text{Sr}_2\text{YRuO}_6$  ( $T_N = 32$  K) and  $\text{Sr}_3\text{LiRuO}_6$  ( $T_N = 90$  K). Indeed, the value of ruthenium in the study of exotic magnetism is enhanced by the fact that the element can adopt many oxidation states;  $\text{Ru}^{2+}$  ( $4d^6$ ,  $S=0$ ),  $\text{Ru}^{3+}$  ( $4d^5$ ,  $S=1/2$ ),  $\text{Ru}^{4+}$  ( $4d^4$ ,  $S=1$ ) and  $\text{Ru}^{5+}$  ( $4d^3$ ,  $S=3/2$ ), thus allowing the possibility of observing both quantum magnetism (for smaller spin values) and pure classical magnetism (for larger spin values) and. In this paper we report a detailed investigation of a  $\text{Ru}^{5+}$  system that shows low-dimensional magnetic behaviour, despite having a 3D crystal structure. More specifically, we have studied  $\text{Li}_3\text{RuO}_4$ , a compound which has previously been shown to have interesting structural and magnetic properties [6, 7]. It has been reported to crystallize in the monoclinic space group  $P2/a$  with the possibility of having a one-dimensional magnetic interaction in a real 3D crystal structure as observed in  $\text{Tl}_2\text{Ru}_2\text{O}_7$ . The structure of  $\text{Li}_3\text{RuO}_4$  can be thought of as being derived from the rock-salt structure. It contains isolated zig-zag chains of edge-sharing  $\text{RuO}_6$  octahedra embedded in a matrix of  $\text{LiO}_6$  octahedra. Pseudo-close-packed planes formed of Li cations alternate with planes containing a mixture of Li and Ru cations along the body diagonal of the rock-salt subcell. In a mixed Li/Ru plane, the Ru cations form a zig-zag chain interleaved by Li atoms, as is shown in Fig.1a. This gives strong intra-chain interactions, but weak inter-chain interactions, resulting in pseudo-1D magnetic interactions between the Ru ions: the nearest-neighbour (NN) Ru-Ru distance in the chain is 2.99 Å. The next-nearest-neighbour (NNN) distance in the chain is 5.10 Å and the distances between the chains along the b-axis are

4.99 Å and 5.85 Å. The 1D nature of magnetism in  $\text{Li}_3\text{RuO}_4$  is hinted at by the temperature dependence of the magnetic susceptibility [6], which exhibits a broad peak at 50 K and strong enhancement in the field cooled data below 10 K (the origin of the latter is not clear, but could be due to small impurity).

Recent numerical studies have concentrated on investigations of  $S=3/2$ , 2 and  $5/2$  systems in order to understand the cross-over from quantum to classical behaviour [8]. However, in a real  $S=5/2$  system the temperature range over which the system shows quantum effects is expected to lie well below  $T_N$ . Experimentally, it has been shown, using inelastic neutron scattering, that an  $S=2$  system,  $\text{CsCrCl}_3$ , behaves classically above  $T_N$  (16 K) [9]. However, recent studies of one-dimensional (1D) antiferromagnets have demonstrated the quantum nature of the spin dynamics in  $S=1/2$  and  $S=1$  chains [10-14]. Thus  $\text{Li}_3\text{RuO}_4$  with  $S=3/2$  is an ideal system to investigate the crossover from the classical to quantum regime. The present study establishes the existence of an antiferromagnetic ground state for  $\text{Li}_3\text{RuO}_4$  before going on to characterize the magnetic excitations in  $\text{Li}_3\text{RuO}_4$ , using inelastic neutron scattering to investigate the low-dimensional nature of the magnetism. The study reveals three clear magnetic excitations below the 3D magnetic ordering temperature,  $T_N=40$  K, and diffuse scattering persisting up to as high as 290 K. We present a classical, theoretical model, which explains the observed magnetic excitations in our powder sample of  $\text{Li}_3\text{RuO}_4$ . The simulation allows us to estimate the three exchange constants,  $J_1$ ,  $J_2$  and  $J_3$  between Ru spins within a chain (intra-chain) and a fourth one  $J_b$  between the chains (inter-chain), see Fig. 1b. We also present an analysis of the temperature dependence of the linewidths and intensities of the excitations and compare them with those observed in other low-dimensional magnetic systems.

## 2. Experimental details

The powder sample of  $\text{Li}_3\text{RuO}_4$  that has been described previously [6] was used in this study. The GEM diffractometer at ISIS has high neutron flux and large detector coverage and hence was ideal for the present study. The sample was cooled to 10 K inside a closed cycle refrigerator (CCR) mounted on the GEM diffractometer at the ISIS pulsed neutron and muon source at the Rutherford Appleton Laboratory, UK and diffraction patterns were collected at several temperatures between 10K and 70 K with a longer counting time (about 6 hours) for 10 K and 70K. The heat capacity was measured using a physical property measurements system (PPMS), supplied by Quantum Design. Part of the sample was pressed into a pellet and a small piece (~8 mg) was mounted in the heat capacity rig using a tiny amount of N-grease. The temperature dependence of the heat capacity was measured from 2 K to 300 K.

The muon spin rotation ( $\mu\text{SR}$ ) measurements were carried out in longitudinal geometry using the  $\mu\text{SR}$  spectrometer at ISIS between 2 K and 70 K. The powder sample was mounted on a silver (Ag) sample holder to reduce background and it was cooled down to 2 K in a standard helium cryostat. Any muons implanting on the Ag sample holder would cause a small time independent background. We carried out inelastic neutron scattering experiments on a powder sample (7 g) of  $\text{Li}_3\text{RuO}_4$  to determine the dynamical scattering function  $S(Q, \omega)$  of the  $S=3/2$ , 1D-zig-zag chain Heisenberg antiferromagnet. The scattering function  $S(Q, \omega)$  was measured between 5 K and 300 K on the time-of-flight chopper spectrometer, HET, also at ISIS. The measurements were carried out using incident neutron energies of 18 and 35 meV with instrumental resolutions of 0.69 meV and 1.19 meV at the elastic position of the 4 m detector bank of HET, respectively. The observed

scattering intensity from  $\text{Li}_3\text{RuO}_4$  was converted into an absolute unit of mb/sr/meV/f.u. by normalizing to the measured intensity from a standard vanadium sample with identical energy settings. The sample was cooled down to 5 K under He-exchange gas in a top loading CCR.

### **3. Results and discussion**

#### **3.1 Heat capacity measurements**

A sharp transition is observed in the heat capacity at 38 K (Fig. 2) with a jump of  $12.4 \text{ (J mol}^{-1} \text{ K}^{-1})$ , which is indicative of a transition to 3D order at 38 K. No detectable transition at lower temperature is observed. Without the heat-capacity data from a proper phonon reference compound it was not possible to analyse the heat capacity data below the magnetic ordering temperature to check whether a gap is present in the magnon spectrum. The observed value of the heat capacity at 300 K is  $202 \text{ J mol}^{-1} \text{ K}^{-1}$ , which is in good agreement with that expected from the lattice contribution  $199.5 \text{ J mol}^{-1} \text{ K}^{-1}$  for  $\text{Li}_3\text{RuO}_4$  [15].

#### **3.2 Neutron Diffraction study**

Rietveld refinement of the structure of  $\text{Li}_3\text{RuO}_4$  at 70 K, using data from 5 detector banks (banks 2 to 6, scattering angles  $2\theta = 18^\circ, 35^\circ, 64^\circ, 91^\circ$  and  $154^\circ$ ) of the GEM diffractometer resulted in a model that is consistent with previously published results [6] (space group P2/a with  $a=5.0987(21) \text{ \AA}$ ,  $b=5.847(2) \text{ \AA}$ ,  $c=5.0991(19) \text{ \AA}$  and  $\beta=110.03(1)^\circ$ ). As previously, a small amount of  $\text{Li}_2\text{CO}_3$  (~3%), one of the starting materials for the synthesis, was detected in the sample. Diffraction data from the high-resolution bank (bank-6) are presented along with the calculated pattern in Fig.3 ( $R_f = 3.03$  for the  $\text{Li}_3\text{RuO}_4$  phase). Data with good counting statistics were also

collected at 10 K, the base temperature of the CCR, but, due to time constraints, the temperature evolution of the diffraction pattern between 15 K and 40 K was obtained using shorter data collection times. A difference plot (not shown) between the 70 K and 10 K data from bank2 (18°) showed that no extra Bragg peaks appear at low temperature. However, the intensity of some of the nuclear peaks does increase on cooling. The Q-dependence of the extra Bragg scattering is typical of a form factor and its appearance coincides with the disappearance of the paramagnetic scattering at very low q (see inset of Fig. 4), indicating that it is magnetic in origin and that the system orders with a k=0 structure. A magnetic contribution to the scattering is clearly visible at 4 positions: strong extra scattering is observed at 5.85 Å (0 1 0) and 3.70 Å (0 -1 1, 0 1 1, 1 1 0 and 1 -1 0), whilst smaller extra contributions are seen around 4.79 Å (001 and 100), and 3.40 Å (-1 -1 1 and -1 1 1). It should be pointed out that a previous low-temperature neutron diffraction study did not detect any evidence of long-range magnetic ordering [6], due to the magnetic intensity being very weak. The extra flux on GEM compared to that on the instrument used in the previous study made it possible to identify the magnetic Bragg peaks. In order to solve the magnetic structure uniquely, we carried out a symmetry analysis of the Ru atom at the 2e position (1/4, 0.8645, 0) with k=0 which reveals that 4 modes are possible according to the irreducible representation of the wave-vector

$$\Gamma_{mag} = \Gamma_1 + \Gamma_2 + 2\Gamma_3 + 2\Gamma_4$$

$\Gamma_1$  ( $\Gamma_2$ ) corresponds to ferromagnetic (antiferromagnetic) order with the moments aligned along the b axis. For both of these modes, there can be no magnetic contribution to the 010 peak reflection. As this is the strongest contribution observed experimentally, these two modes can clearly be discarded.  $\Gamma_3$  ( $\Gamma_4$ ) corresponds to ferromagnetic (antiferromagnetic) ordering with the atomic magnetic moments confined to the ac-plane. Although it is harder to distinguish between

these remaining two modes, using  $\Gamma_4$  rather than  $\Gamma_3$  reduces the intensity around  $4.79\text{\AA}$  which is very weak experimentally. Given the AF character of the susceptibility and the fact that when using  $\Gamma_3$  the value of  $R_{\text{mag}}$  increases, the AF model is favoured. In order to determine unambiguously the moment direction, it would be very useful to obtain single crystals so that further magnetic susceptibility or/and neutron scattering measurements could be performed. Rietveld analysis of data collected at 10 K using bank 2 (presented in Fig.4) and bank 3, using the FullProf program [16], gave magnetic R-factors of 7.7 and 8.2 respectively; the proposed  $\Gamma_4$  magnetic structure is presented in Fig.1b. Values of the moments are :  $M_x = 1.93(04) \mu_B$ ,  $M_z = -0.19(06) \mu_B$  , giving a total magnetic moment of  $2.00(07) \mu_B$ , which is close to the values measured previously in other mixed-metal oxides containing the  $\text{Ru}^{5+}$  cation.

### 3.3 Zero-field muon spectroscopy study

The MuSR spectrum collected at zero applied field at 1.5 K is presented in Fig.5. It is immediately apparent that coherent frequency oscillations, characteristic of 3D long-range magnetic ordering are present. Furthermore, the observation of beating indicates that more than one muon frequency is present in the sample. Indeed, the field distribution, determined using a maximum entropy method, reveals the presence of two field components, very close to each other, confirming two muon frequencies. The data are best described by the following equation:

$$A(t) = \sum_{i=1}^2 \left( a_i \cos(\omega_i t + \varphi) \exp(-(\sigma_i t)^2) + a_i' \exp(-\lambda_i t) \right) + a_{\text{bgd}}$$

(1)

where  $\omega_i$  are the frequencies of the oscillations (we used the results from the maximum entropy

as starting parameters for each temperature),  $a_i$  are the amplitudes of each oscillating component (approximately equal) whilst  $a_i'$  and  $a_{\text{bkgd}}$  are the lorentzian and background amplitudes. The  $\sigma_i$  are the Gaussian damping of the oscillations while  $\lambda_i$  are the Lorentzian relaxations. The temperature dependence of the two muon frequencies is presented in Fig. 6, together with that of the 3.7 Å Bragg peak from the ND study. Each muon frequency was fitted to the standard phenomenological equation for temperature evolution of the order parameter [17, 18].

$$\omega = \omega_o \left( 1 - \left( \frac{T}{T_N} \right)^\alpha \right)^\beta \quad (2)$$

We have carried out fits with two methods: (I) with  $\alpha=1$  (fixed) over the temperature range  $31 < T/K < 40$  and, (II) with  $\alpha$  as a variable over the full temperature range ( $10 < T/K < 40$ ). The extracted parameters from the least squares fit are: for method-I with  $\alpha=1$  (fixed) 11.32 MHz and 11.71 MHz for  $\omega_o$ , 38.99 K and 38.86 K for  $T_N$  and 0.32 and 0.31 for  $\beta$  and for method-II, 8.61 MHz and 8.91 MHz for  $\omega_o$ , 39.02 K and 38.91 K for  $T_N$ , 0.32 and 0.36 for  $\beta$  and 3.15 and 3.19 for  $\alpha$ . From the high-temperature value of the muon relaxation rate, it is possible to predict where the muon is located and, as expected, it is close to an oxygen atom. We have used this information together with the magnetic structure determined from our ND data to predict what the magnetic field is likely to be at the muon site, which indeed reveals two sites seeing two very slightly different fields.

### 3.4 Inelastic neutron scattering study

Before discussing the inelastic spectra, it is worth pointing out that, as seen in our ND

measurements, discussed above, the HET data with  $E_i=35$  meV and 18 meV at 5 K also reveal extra magnetic intensity on the Bragg peaks in the elastic channel at  $Q=1.07$  and  $1.71 \text{ \AA}^{-1}$  (covered in 35 meV data, see Fig. 9), compared with the data for  $T \geq 50$  K. This further confirms the 3D magnetically-ordered ground state of  $\text{Li}_3\text{RuO}_4$ . The Q-integrated data, Fig. 7, show, surprisingly, three well-defined peaks, which we shall call the low-, middle- and high-energy peak, respectively. They all have a finite energy width even at the lowest temperature,  $T=5$  K. The width and the intensity of the peaks develop quite differently as a function of temperature. The most striking result from the Q-resolved inelastic data is the presence of the two well-resolved spin-wave modes emerging out of the two AF zone centres with  $Q=1.07$  and  $1.71 \text{ \AA}^{-1}$  at 5 K (see Figs. 8 and 9), corresponding to  $[0\ 1\ 0]$  and  $[0\ 1\ 1]$  or  $[1\ 1\ 0]$  magnetic Bragg peaks. Fig.8 (a-d) shows the colour contour maps of the scattering intensity, plotted as energy transfer versus momentum transfer, with  $E_i = 18$  meV at selected temperatures: 5, 40, 50 and 290 K. Fig. 8a shows two well-defined spin waves modes at 5.5 and 8.5 meV at 5 K in addition to a weak excitation near 2 meV. Interestingly the intensity of the 8.5 meV peak is stronger at lower Q, while the intensity of 5.5 meV peak is very weak at the lowest Q. The energy maximum of the middle-energy and high-energy modes is nearly Q independent, while that of the low energy mode near  $\sim 2$  meV reveals a slight increase in energy with increasing Q: the maximum occurs at 2.9 meV for  $Q = 1-1.5 \text{ \AA}^{-1}$ . Owing to the instrumental resolution and strong elastic peak intensities, it is not possible to determine conclusively whether the width of the 2 meV peak changes with Q or not.

Fig.7 (a-j) shows the Q-integrated intensity versus energy cuts from  $E_i=18$  meV data at various temperatures between 5 K and 290 K. It is interesting to note from Fig. 7(a-j) that when the

temperature is raised from 5 K to 36 K, the spin-wave energy of the modes at  $\sim 5.5$  and 8.5 meV does not change very much. A similar weak temperature dependence of the spin-wave energies has also been observed for the spin=1/2 1D Heisenberg antiferromagnet,  $\text{CuCl}_2 \cdot 2\text{N}(\text{C}_5\text{D}_5)$  [19]; it should be noted, however, that for this compound the excitations broaden rapidly. In contrast, the intensity of our high-energy mode in  $\text{Li}_3\text{RuO}_4$  decreases strongly with increasing temperature (see Figs.7 and 8) and at 40 K ( $T_N$ ) the high-energy branch has completely disappeared. On the other hand, despite the renormalization of the energy observed near  $T_N$ , the middle-energy mode does not disappear above  $T_N$ . We have observed a clear inelastic diffuse scattering peak at 50 K, which persists up to 148 K with a nearly temperature-independent position near  $\sim 4$  meV. Above 148 K, the data could be well fitted with either an inelastic peak or by using only a quasi-elastic peak (Figs.7 and 8).

The temperature dependence of the intensity of the middle- and high energy modes between 5 K and  $T_N$  of  $\text{Li}_3\text{RuO}_4$  is interesting. It remains almost constant up to 20 K and then decreases to zero at 40 K for the high energy mode, but increases gradually with temperature up to  $T_N$  then decreases slowly above it for the middle-energy mode. Our model discussed below offers an explanation for the different temperature dependence of the intensity of the middle- and high-energy modes in  $\text{Li}_3\text{RuO}_4$ . The presence of spin waves above  $T_N$  in  $\text{Li}_3\text{RuO}_4$  is reminiscent of other low dimensional systems, such as  $\text{CsVCl}_3$ , which exhibits 1D magnetism [20]. The spin dynamics of  $S=3/2$  1D Heisenberg antiferromagnet  $\text{CsVCl}_3$  have been investigated above and below the 3D magnetic ordering temperature  $T_N=13.3$  K [20]. This compound also exhibits a well defined spin wave mode above  $T_N$ , which has been attributed to 1D-type magnetic interactions based on classical spin wave theory [21]. We therefore attribute the presence of the middle-energy mode

above  $T_N$  in  $\text{Li}_3\text{RuO}_4$  to the low dimensionality (quasi 1D) of the magnetic interaction between the Ru ions along the zig-zag chain.

## 4. Spin wave analysis

### 4.1 Model and dispersion relation

We present an analysis of the inelastic neutron scattering data collected on  $\text{Li}_3\text{RuO}_4$  using two simple spin-wave models. Although the system is almost one dimensional (1D), we use standard, classical spin-wave theory for 3D, weakly-interacting zig-zag linear chains running in the  $a$ -direction in the pseudo-close-packed ( $a$ - $b$ ) plane of  $\text{Li}_3\text{RuO}_4$  (Fig.1b). We use two sublattices, A and B, for the spin up and down. The lattice vector  $\mathbf{b}$  connects the spins on the same sublattice on adjacent chains, and  $\mathbf{a}$  connects those on the same sublattice along the chain (See Fig.1b). We assume a simple AF ground state with the spins in the  $a$ -direction (taken as a quantization axis), along one of the zig-zag bonds, see Fig. 1b. This direction may be stabilized by the presence of a small uniaxial anisotropy; however the actual direction is not important in the present analysis. Usually, antiferromagnets have two degenerate spin wave branches, whereas in the presence of a planar anisotropy the branches split up, in particular at low energy. Since there is no evidence for that, we assume no planar anisotropy. We analyse the observed low-temperature spin-wave data with two very simple models. The powder data washes out a number of details in the dispersion relation, hence only a minimal number of interactions can be determined. Consequently we have used interactions in the  $ab$ -plane only and have ignored the interactions between the planes, although our spin-dimer analysis (not discussed here) and density functional theory (DFT) calculations [22] indicate that they are not negligible. Both models have three interactions  $J_1$ ,  $J_2$ ,  $J_3$  along the chain and a weak effective interaction between the neighbouring chains. It represents

the sum of all possible interactions both within the ab-plane and between the planes. For simplicity, we take this to be the in-plane inter-chain interaction between opposite sublattices (see Fig.1b.). For the first model (model-1), we assume a very small (or no) axial anisotropy and an antiferromagnetic  $J_b$  interaction between the chains. This model, which is the most natural, if the system was a normal 3D antiferromagnet, gives rise to a very small energy gap at  $q=0$ . However, if the 1D nature plays a large role there might be a gap. To account for this possibility, we consider as a second case (model-2) a larger axial anisotropy, which effectively can simulate such a gap for the 1D chain dispersion relation, while we then assume an ferromagnetic  $J_b$  coupling between the chains.

The anisotropy and the exchange interaction between the spins are given by the following Hamiltonian

$$H = -\sum_{\langle ij \rangle} J_{ij} (\mathbf{S}_i^A \cdot \mathbf{S}_j^A + \mathbf{S}_i^B \cdot \mathbf{S}_j^B) - \sum_{\langle ij \rangle} J'_{ij} (\mathbf{S}_i^A \cdot \mathbf{S}_j^B + \mathbf{S}_i^B \cdot \mathbf{S}_j^A) - \sum_i [D (S_i^z)^2 - P (S_i^y)^2] \quad (3)$$

Here the first term represents the intra-chain interaction (summing over pairs, i.e.  $J_1$ ,  $J_2$  and  $J_3$ ) with  $\mathbf{S}^A$  and  $\mathbf{S}^B$  representing the  $S=3/2$  spin operators on two chains. The second term represents the inter-chain interactions (i.e.  $J_b$ ), while the third term presents the usual single-ion anisotropy:  $D$  is an easy-axial anisotropy and  $P$  is a planar anisotropy. For an antiferromagnet the dispersion relations are given by [23]

$$E_q^\pm = (A_q^2 - C_q^2 - |B_q \pm D_q|^2)^{1/2} \quad (4)$$

We denote the wave vector  $\mathbf{q}$ , with the length  $|\mathbf{q}|=Q$ . The above model gives

$$\begin{aligned} A_{\mathbf{q}} &= S(J_0 - J_{\mathbf{q}} + J'_0) + 2D(S-1/2), \\ B_{\mathbf{q}} &= P(S-1/2), \quad C_{\mathbf{q}}=0, \\ D_{\mathbf{q}} &= S J'_{\mathbf{q}} \end{aligned} \quad (5)$$

Only in presence of an anisotropic exchange (dipolar) interaction is  $C_{\mathbf{q}}$  different from zero. The Fourier-transformed interaction constants are

$$\begin{aligned} J_{\mathbf{q}} &= 2J_2 \cos(\mathbf{q} \cdot \mathbf{a}), \\ J'_{\mathbf{q}} &= -[(2J_1 + 4J_b \cos(\mathbf{q} \cdot \mathbf{b})) \cos(\mathbf{q} \cdot \mathbf{a}/2) + 2J_3 \cos(3\mathbf{q} \cdot \mathbf{a}/2)] \exp(i\mathbf{q} \cdot \mathbf{b}/4) \end{aligned} \quad (6)$$

Here  $J_1, J_2, J_3$ , are interactions between neighbours 1-3 along the zig-zag chain, and  $J_b$  is the interaction between the chains in the a-b-plane (at distance 4.98 Å) as mentioned previously. Since that interaction is very weak, we consider it for simplicity as an effective interaction between linear chains. We neglect a possible interaction between the chains in different planes. Clearly, if there is no planar anisotropy,  $P=0$  and  $B_{\mathbf{q}}=0$ , we see from Eq.(4), that the complex part of  $J'_{\mathbf{q}}$  does not play a role and the branches are degenerate with

$$E_{\mathbf{q}} = E_{\mathbf{q}}^{\pm} = S[(J_0 + J'_0 + Ds - J_{\mathbf{q}} - |J'_{\mathbf{q}}|)(J_0 + J'_0 + Ds - J_{\mathbf{q}} + |J'_{\mathbf{q}}|)]^{1/2} \quad (7)$$

where  $s = (1 - S/2)$ . The  $\mathbf{q}$ -dependent intensity from both branches is then simply proportional to  $I_{\mathbf{q}} = A_{\mathbf{q}}/E_{\mathbf{q}}$ . In the following powder averaging we neglect the weak dependence  $(1+(\boldsymbol{\kappa} \cdot \mathbf{m})^2)$  on the

relative direction of the unit vectors of the scattering vector,  $\mathbf{\kappa}$ , and the sublattice magnetization,  $\mathbf{m}$ . The dispersion and the intensity are of course strongly dependent on the  $\mathbf{q}$ -direction. As our neutron measurements have been carried out on a powder sample, we have averaged over all  $\mathbf{q}$ -directions to obtain the magnon density of states. The simulated spectra do have peaks where the dispersion is flat. Interestingly three such peaks are observed in the Q-integrated simulated intensity (Fig. 10a-d). This can be accounted for by the simple model using the set of parameters

$$\{J_1, J_2, J_3, J_b, D\} = \{-3.3(1), -1.4(1), -1.2(1), -0.010(1), 0.0005(5)\} \text{ meV} \quad (8)$$

It was not possible to do a least-squares-fit to the data because the fit involves not only the dispersion relation, but also the intensity, which was measured on a powder sample. However, by exploring the parameter space the error bars are estimated as indicated (referring to the last digit). The parameters  $J_1, J_2, J_3$  are determined by the middle- and high-energy peaks plus the fact that the intensity of the upper peak is the highest. It is not possible to account correctly for all these features by using just  $J_1, J_2$ . This is not a strong condition, hence the parameters are correlated – and error bars should be understood accordingly. Further,  $J_b$  is determined by the lower peak energy at 2 meV. It corresponds to the zone-boundary in the b-direction, perpendicular to the chain.  $J_b$  is an effective parameter representing the overall interaction between the spin chains. The calculations indicate there maybe further small interactions. The anisotropy can be chosen arbitrarily (small), but is useful for stabilizing the ground state. The determined parameters yield a mean field Néel temperature of  $T_N^{\text{MF}} = 90$  K. As expected in the low dimensional system the actual 3D ordering temperature,  $T_N = 40$  K, is much reduced due to fluctuations. Similarly, we can calculate the Curie-Weiss temperature  $\Theta_{\text{cal}} = -171$  K, which is intermediate between the

experimentally determined values. ( $-137$  K in ref. [6],  $\Theta_{\text{exp}} = -231$  K in ref [7]). The quasi 1D nature of the magnetic interaction between the Ru spins is apparent along the zig-zag chain, with the strong intra-chain NN antiferromagnetic interaction  $J_1$ , the weaker  $J_2$ , and the weak antiferromagnetic interaction,  $J_3$  plus the hundred-fold weaker AF inter-chain interaction  $J_b$  (see Fig.1). It is interesting to note that these values of the exchange parameters as well as their sign are in excellent agreement with those estimated from DFT calculations using 1D model  $J_1$  (in meV) =  $-4.49$ ,  $J_2 = -1.59$ ,  $J_3 = -0.98$ ,  $J_b = 0.0$  [22], indicating the quasi-1D nature of the magnetism of  $\text{Li}_3\text{RuO}_4$  (see below for details).

The calculated Q-integrated intensity is shown in Fig. 10a. The middle energy peak at  $5.5$  meV corresponds to the zone-boundary in the a-direction, and the high energy peak at  $8.5$  meV to a region near half the zone-boundary. This is evident from the density plot of the intensities in the  $(Q, E_q)$  plane, Fig 10c. One notices the contours of the dispersion relation along the chain ( $5.5$  meV and  $8.5$  meV peaks) and of that perpendicular to the chain ( $\sim 2$  meV peak). The powder averaging gives the maximum intensities along three almost Q-independent bands. The high-energy peak has maximum intensity at lower Q, whereas the middle-energy peak picks up at around the zone boundary ( $Q=1.07 \text{ \AA}^{-1}$ ) and beyond. This is in perfect agreement with the observed intensity behaviour in our powder sample of  $\text{Li}_3\text{RuO}_4$ . In this model-1 (for  $D=0$ ) there is no energy gap at  $Q=0$  for the dispersion of the 1D chain.

Alternatively, we can fit the two higher-energy excitations equally well with a second model-2, which has an energy gap for the linear chain at  $q=0$ . This can be done in the simplistic model by choosing a larger  $D = 0.05$  meV and a positive interaction between the chains  $J_b = 0.008$  meV

(and the above values of  $J_1, J_2, J_3$ ). The results for the  $(Q, E_q)$  intensity colour contour plot are given in Fig. 10b and for the Q-integrated intensity of the magnon density of states versus energy transfer is shown in Fig. 10d. The only change observed in model-2 compared to model-1 is the inverted low energy ( $\sim 2$  meV peak) dispersion, but the high-energy response (5.5 meV and 8.5 meV) remains the same in both the models. The parameters determined using the model-2 yield mean-field Néel and Curie temperatures very similar to those calculated using model-1.

The DFT calculations reveal that all the interactions are antiferromagnetic [22], in support of model-1. The upper energy part of the dispersion along the chain is already well determined in the present study. Further detailed measurements on a single-crystal sample of  $\text{Li}_3\text{RuO}_4$  at low energies would be highly desirable to make a clear distinction between the alternative models proposed here as well as to find out whether any other exchange interactions, which are not considered here, are significant. In the analysis, we have not considered the full quantum nature of the 1D system. The obtained parameters are therefore effective and may have to be scaled ( $\pi/2$  is the scale factor [24] for a linear  $S=1/2$  chain) – but the relative magnitudes should remain the same.

#### **4.2 Temperature dependence of intensity and width**

The temperature dependences of the peak intensity and width of the various modes discussed below, are both surprising and interesting. The middle- and lower-energy peaks remain intense up to temperature much larger than  $T_N$ . We now realize these correspond to zone-boundary excitations. These short-wavelength excitations are known to persist even in the disordered state with strong short-range order [23]. The high-energy peak disappears at  $T_N$ , which is consistent

with the longer-wavelength nature of that excitation (being from the middle of the zone). Even at the lowest temperatures, there is a “linewidth” due to the powder averaging, as seen in Fig. 10c and 10d in comparison with Fig. 7. A more detailed calculation is required in order to account for the detailed behaviour of the intensity, energy and linewidth. However, our simple model-1 accounts for all of the major features observed in this inelastic study of the powder sample of  $\text{Li}_3\text{RuO}_4$ .

Hereafter we present an analysis of the experimentally-observed spin-wave linewidth and intensity in  $\text{Li}_3\text{RuO}_4$  sample. The intrinsic spin-wave linewidth, which is the inverse of the spin-wave lifetime, provides valuable information on the magnon-magnon scattering mechanism. It is directly associated with the relevant damping mechanisms and reflects how the quantized magnons interact with other scattering processes. We have therefore carried out a detailed analysis of spin-wave linewidth using a Lorentzian form of the spectral function convoluted with the instrument resolution (this includes effectively the “linewidth” due to the powder averaging). The instrument-resolution parameters were estimated first by fitting the identical cuts/spectra from monochromatic vanadium runs measured with identical conditions. The following form of  $S(Q, \omega)$  was used in our data analysis:

$$S(Q, \omega) = \left( \frac{\omega}{1 - \exp(-\hbar\omega/k_B T)} \right) F^2(Q) \frac{1}{\pi} \sum_i (\chi_i) \left( \frac{\Gamma_i}{(\hbar\omega - \hbar\omega_{i0})^2 + \Gamma_i^2} + \frac{\Gamma_i}{(\hbar\omega + \hbar\omega_{i0})^2 + \Gamma_i^2} \right), \quad (9)$$

where  $F^2(Q)$  is the  $\text{Ru}^{5+}$  form factor taken from ref. [25],  $\Gamma_i$  is the linewidth and  $\omega_{i0}$  is the position of the peak and  $\chi_i$  is the static susceptibility, which is proportional to the integrated intensity of

the peak. We have analysed both the 35 meV (at 5K) and the 18 meV data at all temperatures between 5 K and 300 K. The quality of the fit to 18 meV data can be seen in Fig. 7 and the fit parameters plotted as a function of temperature are shown in Fig. 11. In addition to the middle-energy and high-energy modes, the 18 meV data show a better fit near the elastic tail, when a low energy peak near 2 meV is added: we attribute the origin of this peak to the low-energy mode arising from the weak inter-chain interactions as discussed above. The data between  $T > T_N$  and 291 K were fitted with two methods, (i) a broad inelastic peak near 4 meV and, (ii) only a quasielastic peak centred at zero energy transfer. The data between  $T > T_N$  and 148 K can be fitted better with the inelastic peak than with the quasielastic peak, but at 207 K and 291 K both the methods gave equally good fits.

First we discuss the absolute value of the linewidth at 5 K for both the middle-energy (5.5 meV) and high-energy (8.5 meV) modes. Both have larger widths than are accounted for by the powder averaging. The linewidth of the middle-energy mode at 5.5 meV is 0.65 meV, which is 11.8% of the energy of the mode, on the other hand the linewidth of the high-energy mode at 8.5 meV is 0.29 meV, which is 3.4% of the energy of the mode. These values are much smaller than those found in the bilayer manganite, 40% for middle-energy (at 6.2 meV) and 29% for high-energy (at 12 meV) modes, although in both systems the middle-energy mode is much broader than that of high-energy mode [26]. It is to be noted that the width of the high-energy mode near the zone boundary is larger than that of the middle-energy mode in the manganites [27].

Now we discuss the temperature dependence of the spin-wave linewidth in the AF-ordered state. We have used two methods to analyse the temperature dependence of the linewidth below  $T_N$ ; (I)

using a power law behaviour  $\Gamma(T) = a_1 * T^n + b_1$  [28], and (II) thermally activated relaxation rate,  $\Gamma(T) = a_2 * \exp(-\Delta/k_B T)$  [29]. The fit to the middle-energy linewidth between 5 K and 40 K with all three variables,  $a_1$ ,  $n$ ,  $b_1$  was good with  $n = 2.9(8)$ . However, there was a large error on the estimated value of  $a_1$ . Hence, we fixed the value of  $n = 3$  and fitted both the data of middle-energy and high-energy modes; the fits are shown by the solid line in Fig. 11 (middle). It is interesting to compare this exponent value with  $n = 3.29$  observed for the Heisenberg antiferromagnet  $\text{RbMnF}_3$  [28].  $n = 3$  is also predicted by the theoretical spin-wave calculations based on the hydrodynamics theory for the four-magnon interaction for some range of energy and temperature by Harris et al [30]. Furthermore, the analysis based on the thermally activated relaxation method-II (see dotted line in Fig. 11) also gave an equally good fit for the middle-energy linewidth compared with as method-I, but not to the high-energy linewidth near  $T_N$ . The quality of the fits can be seen in Fig. 11 (middle) dotted line.

There are many sources for linewidth broadening and its temperature dependence: (i) magnon-phonon scattering, (ii) magnon-electron, and (iii) magnon-magnon scattering. We have not observed any sign of strong phonon peaks, close or overlapping the energy range of the spin-wave branches, hence we rule out the possibility of magnon-phonon interaction. Although we do not have resistivity data on this compound at present, by considering the general behaviour of antiferromagnetic transition-metal oxide-systems, we would expect  $\text{Li}_3\text{RuO}_4$  to behave as an insulator at low temperatures. This also suggests that magnon-electron coupling should be weak. Thus, it is reasonable to assume that magnon-magnon scattering, possibly four-magnon scattering, is playing an important role in the damping of the spin wave in  $\text{Li}_3\text{RuO}_4$ . It should be noted that the four-magnon scattering cross-section is very weak compared to the single-magnon

scattering process, hence it would be difficult to observe a direct energy scale and intensity associated with this process in the powder sample. Similar linewidth broadening by four magnon-processes has been reported for the antiferromagnet  $\text{RbMnF}_3$  [28].

Next, we discuss the renormalization of spin wave energy. We have analysed the temperature dependence of the energy of both middle-energy (at 5.5 meV) and high-energy (at 8.5 meV) model using the following functional form (i.e. simply renormalized according to the magnetization)

$$E = E_1 + E_0 * ([T_N - T] / T_N)^\beta \quad (10)$$

Where  $\beta$  is the critical exponent,  $E_0$  is the magnon energy at  $T=0$  and  $E_1$  is the magnon energy above  $T_N$ . The best fit to the high-energy mode gave  $T_N = 38.93(1.92)$  K,  $\beta_h = 0.044(10)$ ,  $E_{0h} = 8.60(06)$  meV and  $E_{1h} = 0$  meV. For fitting the middle-energy mode energy we kept  $T_N = 38.93$  K fixed from the previous fit and  $E_{1m} = 3.61$  meV fixed from the 50 K data, the best fit gave the value of  $\beta_m = 0.29(07)$ ,  $E_{0m} = 2.02(08)$  meV. This analysis shows that the two excitations have very different temperature-dependent behaviour. Only the renormalization of the middle excitation seems to qualitatively follow the order parameter. We would like to mention here the value of  $\beta$  observed in other low dimensional systems:  $\beta = 0.16(0.01)$  has been observed for the 2D spin  $S=5/2$  square-lattice Heisenberg antiferromagnet  $\text{Rb}_2\text{MnF}_4$  [31],  $0.15(0.01)$  for both the bilayer  $\text{K}_3\text{Mn}_2\text{F}_7$  and single layer  $\text{K}_2\text{MnF}_4$ ,  $0.138(0.004)$  for  $\text{K}_2\text{NiF}_4$  [32] and  $0.21(0.01)$  for bilayer manganites,  $\text{La}_{1.2}\text{Sr}_{1.8}\text{Mn}_2\text{O}_7$  [26].

Finally, we discuss the correlation length and short-range correlations observed above  $T_N$  in

$\text{Li}_3\text{RuO}_4$ . The data in Figs 7 and 8 clearly reveal the presence of short-range diffuse scattering at 50 K near the antiferromagnetic zone centre. In order to estimate the correlation length, we have analysed the difference data, 50 K – 5K, energy integrated  $Q$ -cut, using the following functional form

$$I(Q) \sim H / ((Q-Q_0)^2 + \kappa_p^2) + bg \quad (11)$$

The best fit gives a value of  $\kappa_p = 0.36$  (0.08), corresponding to a correlation length  $\xi = 1 / \kappa_p = 2.79(60)$  Å with  $H = 1.67(0.85)$ ,  $Q_0 = 1.10(0.02)$  and  $bg = 3.5$  (1.5). The quality of the fit can be seen in Fig.12. A different estimate of the correlation length calculated by fitting a Gaussian function to  $I(Q)$ , gives  $\xi \sim 2.0 / (2.354 * \sigma) = 2.97(45)$  Å. These analyses reveal that above  $T_N$ , we observe the presence of short range correlations, only over a distance of the NN Ru-Ru atoms, which are AF in nature. The correlation time ( $\tau$ ) of the short-range fluctuations was estimated by fitting a quasi-elastic Lorentzian function,  $\tau = \hbar / \Gamma$ , to the  $Q$ -integrated energy cut at 50 K, giving  $\tau = 1.78 \times 10^{-12}$  (s) (and  $1.12 \times 10^{-12}$  (s) at 295 K).

## 5. DFT analysis of spin exchange parameters

In recent years, the energy-mapping analysis based on DFT calculations [33] has been found to give remarkable agreements in determining the relative strengths and the signs of the spin exchange interactions in a variety of transition-metal oxides and hence has provided detailed understanding of their magnetic properties [34-38]. Our DFT evaluation of the spin-exchange interactions of  $\text{Li}_3\text{RuO}_4$  [22] employed the projector augmented wave (PAW) method encoded in the Vienna ab initio simulation package (VASP) [34-36] with the generalized-gradient

approximation (GGA) [37] for the exchange-correlation functional, the DFT plus on-site repulsion  $U$  calculations [38] for the Ru 4d states, and the crystal structure of  $\text{Li}_3\text{RuO}_4$  determined at 70 K. The labelling of the interactions used for the calculations is defined in Fig. 1b. Here we briefly summarize the main outcome of this DFT study relevant for the present spin-wave calculation (for the details of the calculations, see ref. [22]). To check whether or not it is appropriate to use a quasi-1D model for the spin wave analysis, we evaluated the spin exchange parameters of  $\text{Li}_3\text{RuO}_4$  by considering that it is a 3D, 2D or 1D magnetic system. The values of the relevant spin exchange interactions estimated with these models are given in Table-I. Table-I shows that  $J_b$  is strongly antiferromagnetic in both 3D and 2D models, and that  $J_3$  is very weakly antiferromagnetic for the 3D model, but very weakly ferromagnetic for the 2D model. Interestingly, for 1D model,  $J_3$  is strongly antiferromagnetic and is not negligible compared to  $J_1$  and  $J_2$ . More interestingly, the magnitudes and signs of  $J_1$ ,  $J_2$  and  $J_3$  estimated for the 1D model are very close to those estimated from the spin-wave analysis model-1, in strong support of the quasi-1D nature of the interaction in  $\text{Li}_3\text{RuO}_4$ . To further check the 1D nature we simulated the spin wave dispersion using the spin exchange parameters of the 3D model shown in Table-I. This simulation did not explain the intensities of the 5 meV and 8 meV modes and did not give the low energy mode as observed in our inelastic data. These results strongly support the use of the quasi-1D model for the interpretation of the spin wave dispersion relations of  $\text{Li}_3\text{RuO}_4$ .

## 6. Conclusions

We have carried out neutron diffraction,  $\mu\text{SR}$  and inelastic neutron-scattering measurements on  $\text{Li}_3\text{RuO}_4$  to understand the nature of the magnetic ground state in this quasi-1D system. Neutron diffraction and  $\mu\text{SR}$  studies clearly reveal the long range AF magnetic ordering of the Ru

moment with a propagation vector  $k = (0\ 0\ 0)$  below 40 K. Our inelastic neutron-scattering studies reveal the presence of three spin wave modes in  $\text{Li}_3\text{RuO}_4$  below  $T_N = 40$  K: a middle-energy mode at 5.5 meV, a high-energy mode at 8.5 meV, and another low-energy mode at 2 meV arising from the interchain interactions between the Ru atoms. Our theoretical spin wave calculations allow us to estimate the three AF intra-chain interactions [in meV,  $J_1 = -3.3(1)$ ,  $J_2 = -1.4(1)$ ,  $J_3 = -1.2(1)$ ] as well as a much weaker AF inter-chain interaction  $J_b = -0.010(1)$  meV. The estimated values of the intra-chain interactions are in excellent agreement with those calculated using DFT theory for the 1D model, revealing the quasi-1D nature of the magnetism in  $\text{Li}_3\text{RuO}_4$ . Furthermore, above  $T_N$  we have observed diffuse scattering arising from the short range magnetic correlations between the NN Ru ions along the zigzag chains. We have estimated the correlation length,  $\xi \approx 2.9$  Å (and correlation time  $\tau \approx 1.78 \times 10^{-12}$  sec) at 50 K, which is close to 2.99 Å, the distance between the Ru atoms in the edge-sharing  $\text{RuO}_6$  octahedra along the zigzag chain. We also presented the temperature dependence of the linewidth and the intensities of the inelastic modes. The width of the middle-energy mode at 5.5 meV is higher than that of the high-energy mode at 8.5 meV at lowest temperature and the difference increases with increasing temperature. Based on the absence of any obvious phonon modes near 5 meV, and the assumption that  $\text{Li}_3\text{RuO}_4$  exhibits an insulating behaviour like other AF transition-metal oxides, we suggest that the cause of the larger linewidth of the middle-energy mode may be due to magnon-magnon interactions. We expect that the present study will spur further research activity on ruthenates and will prove important in understanding the nature of low-dimensional magnetism in real 3D systems such as  $\text{Na}_3\text{RuO}_4$  [39].

## Acknowledgments

We would like to acknowledge Drs Radu Coldea, Matthew Stone, Chris Stock, Tapan Chatterji, Profs. Alan Tennant, Brian Rainford, Keith McEwen and J.-G. Park for interesting discussions. We thank the ISIS facility for providing us with a beam time at ISIS pulsed neutron source. M.-H. W. thanks the financial support from the Office of Basic Energy Sciences, Division of Materials Sciences, U. S. Department of Energy, under Grant DE-FG02-86ER45259.

**Table- 1:** The spin exchange parameters of the 3D, 2D and 1D spin lattice models from the GGA+U calculations with  $U = 3$  eV. The last column shows the exchange parameters estimated from the spin waves analysis, model-1.

	Ru-Ru ( $\text{\AA}$ )	3D	2D	1D	SW-model-1
$J_1$	2.99	-3.13	-3.22	-4.49	-3.3(1)
$J_2$	5.10	-1.37	-2.16	-1.59	-1.4(1)
$J_3$	7.81	-0.30	+0.17	-0.98	-1.2(1)
$J_b$	4.99	-1.96	-2.51	0.00	-0.010(1)

### Figure captions

Fig.1 (color online): (a) The crystal structure of  $\text{Li}_3\text{RuO}_4$  showing the presence of one-dimensional zigzag chain of Ru atoms along a-axis in  $\text{Li}_3\text{RuO}_4$ . For clarity only the metal atoms are shown, Ru-atoms (large red spheres) and Li-atoms (small light-blue spheres). (b) The view of the magnetic structure in the ab-plane with three intrachain interactions along a-axis ( $J_1$ ,  $J_2$  and  $J_3$ ) and one interchain interaction along b-axis ( $J_b$ ). The moments along c-axis are coupled ferromagnetically. Please note that the moment also has a small component along c-axis, which is not shown in Fig.1b.

Fig.2 (colour online): The heat capacity verses temperature of  $\text{Li}_3\text{RuO}_4$ . The inset shows the heat capacity plot up to 300 K.

Fig.3 (colour online): Rietveld refinement (GEM bank6) for  $\text{Li}_3\text{RuO}_4$  at 70 K. The symbols and line represent the experimental and calculated intensities. The two rows of ticks mark the positions of reflections for the main  $\text{Li}_3\text{RuO}_4$  phase (top) and a small  $\text{Li}_2\text{CO}_3$  impurity (bottom). The line at the bottom of the plot is the difference between the refinement and the data.

Fig. 4 (colour online): Rietveld refinement (GEM bank3) for  $\text{Li}_3\text{RuO}_4$  at 10 K. The conventions are the same as Fig.3 with the third row of ticks indicating the position of the calculated magnetic peaks. The inset shows the data at 70 K in big red circles and at 10 K in small blue squares highlighting the extra intensities on a few Bragg peaks and the loss of paramagnetic scattering at 10 K.

Fig.5 (colour online): Time evolution of  $\mu\text{SR}$  spectrum for  $\text{Li}_3\text{RuO}_4$  at 1.4 K, focusing at short times. The line is a fit as described in the text.

Fig. 6 (colour online):  $\mu\text{SR}$  frequencies extracted from the fits to the depolarisation spectra as a function of temperature (red squares and blue triangles). The lines are fits to equation (2). The solid lines are with  $\alpha=1$  and dotted lines are with  $\alpha$  as a variable. The green circles show the extra intensity on the  $3.7 \text{ \AA}$  neutron diffraction peak (scaled to fit on the same graph).

Fig.7 (colour online) (a-j) Energy transfer versus the Q-integrated intensity of  $S(Q, \omega)$  at various temperatures. The solid and dotted lines represent the fits (see text).

Fig.8 (a-d) (colour online) Colour contour plot of the scattering intensity,  $S(Q, \omega)$ , plotted as energy transfer versus wave vector transfer ( $|\mathbf{q}|=Q$ ) measured using an incident neutron energy of 18 meV at various temperatures from  $\text{Li}_3\text{RuO}_4$ .

Fig.9 (colour online) Colour contour plot of the scattering intensity,  $S(Q, \omega)$ , plotted as energy transfer versus wave vector transfer ( $|\mathbf{q}|=Q$ ) measured using an incident neutron energy of 35

meV at 5 K from  $\text{Li}_3\text{RuO}_4$ .

Fig.10 (colour online) Simulated color contour plot of the powder averaged scattering plotted as energy transfer versus  $Q$  using (a) model-1 with no 1D energy gap at  $q=0$  and with  $D=0$ , and (b) with model-2 having a finite 1D energy gap at  $q=0$  with  $D=0.05$  meV for  $\text{Li}_3\text{RuO}_4$  (see text). (c) and (d) represent the corresponding  $Q$ -integrated intensity plotted as a function of energy transfer for model-1 and model-2 (see text), respectively.

Fig.11 Temperature dependence of the intensity, linewidth and energy position for the middle-energy and high-energy modes as well as 2 meV peak obtained for the fits (see text). The solid and dotted lines show the fits (see text).

Fig.12 Energy integrated  $Q$ -dependence of the temperature difference intensity 50 K – 5K for  $E_i=35$  meV. The line shows the fit (see text).

## References

- [1] P. Khalifah, R. Osborn, Q. Huang, H.W. Zandbergen, R. Jin, Y. Liu, D. Mandrus and R.J. Cava, *Science* **297**, 2237 (2002).
- [2] S. Lee, J.-G. Park, D. T. Adroja, D. Khomskii, S. Streltsov, K. A. McEwen, H. Sakai, K. Yoshimura, V. I. Anisimov, D. Mori, R. Kanno, and R. Ibberson, *Nature Materials* **5**, 471 (2006).
- [3] Y. Maeno, H. Hashimoto, K. Yoshida, S. Nishizaki, T. Fujita, J.G. Bendnorz and F. Lichtenberg, *Nature* **372**, 532 (1994).

- [4] P. Khalifah, K.D. Nelson, R.Jin, Z.Q. Mao, Y. Liu, Q. Huang, Y.P.A. Gao, A.P. Ramirez and R.J. Cava, *Nature* **411**, 669 (2001).
- [5] A. Cllaghan, C.W. Moeller and R. Ward, *Inorg. Chem.* **5**, 1572 (1966); L. Klein, L. Antognazza, T.H. Geballe, M.R. Beasley, A. Kapitulnik, *Physica* **B259-261**, 341 (1999).
- [6] A. Alexander, P.D. Battle, J.C. Burley, D.J. Gallon, C.P. Grey, S.H. Kim. *J. Mater. Chem.* **13**, 2812 (2003).
- [7] M. Soma and H. Sato, *J. Phys. Soc. Jpn.* **75**, 124802 (2006).
- [8] L. Capriotti, R. Vaia, A.Cuccoli and V.Tognetti, *Phys. Rev.* **B58**, 273 (1998); L. Capriotti and R.Vaia, *Phys. Rev.* **B60**, 7299 (1999); N. Hatano and M. Suzuki, *J. Phys. Soc. Jpn.* **62**, 1346 (1993); S. Yamamoto, *Phys. Rev.* **B53**, 3364 (1996).
- [9] S. Itoh, H. Tanaka and T. Otomo, *J. Phys. Soc. Jpn.* **66**, 455 (1997); S. Itoh, H. Tanaka and M. Bull, *J Phys Soc Jpn.* **71**, 1148 (2002).
- [10] S.R. White and I. Affleck, *Phys. Rev.* **B54**, 9862 (1996); N. Maeshima, M. Hagiwar, Y. Narumi, K. Kindo, T.C. Kobayashi and K. Okunishi, *J. Phys. Condens. Matter* **15**, 3607 (2003).
- [11] R.M. Morra, W.J.L. Buyers, R.L. Armstrong, K. Hirakawa, *Phys. Rev.* **B38**, 543 (1988).
- [12] F. D. M. Haldane, *Phys. Lett.* **93A**, 464 (1983); *Phys. Rev. Lett.* **50**, 1153 (1983).
- [13] K. Uchinokura, Y. Uchiyama, T. Masuda, Y. Sasago, I. Tsukada, A. Zheludev, T. Hayashi, N. Miura and P. Böni, *Physica* **B284-288**, 1641 (2000); A. Lappas, V. Alexandrakis, J. Giapintzakis, V. Pomjakushin, K. Prassides and A. Schenck, *Phys. Rev.* **B66**, 14428 (2002); S.M. Rezende and R.M. White, *Phys. Rev.* **B18**, 2346 (1978)
- [14] W. J. L. Buyers, P. M. Morra, R. L. Armstrong, M. J. Hogan, P. Gelrach, and K. Hiraawa, *Rhys. Rev. Lett.* **56**, 3371 (1986); M. Steiner, K. Kakurai, J. K. Kjems, D. Petitgrand, and R. Pynn, *J. Appl. Phys.* **61**, 3953 (1987).

- [15] N.W. Ashcroft and N.D. Mermin, Solid State Physics, W.B. Saunders Company, Philadelphia, page-427 (1976)
- [16] J. Rodriguez-Carvajal, Physica B **192**, 55 (1993)
- [17] A. J. Steele, T. Lancaster, S. J. Blundell, P. J. Baker, F. L. Pratt, C. Baines, M. M. Conner, H. I. Southerland, J. L. Manson, and J. A. Schlueter, Phys. Rev. B **84**, 064412 (2011)
- [18] A. D. Hillier, D. T. Adroja, W. Kockelmann, L. C. Chapon, S. Rayaprol, P. Manuel, H. Michor and E. V. Sampathkumaran, Phys. Rev. B **83**, 024414 (2011)
- [19] Y. Endoh, G. Shirane, R.G. Bergeneau, P.M. Richards and S.L. Holts, Phy. Rev. Lett. **32**, 170 (1974).
- [20] S. Itoh, Y. Endoh, K. Kakurai, H. Tanaka, S. M. Bennington, T. G. Perring, K. Ohoyama, M.J. Harris, K. Nakajima and C.D. Frost, Phys. Rev. B **59**, 14406 (1999).
- [21] S.W. Lovesey, 'Theory of neutron scattering from condensed matter', vol.2, Clarendon, Oxford (1984).
- [22] Won-Joon Son, P. Manuel, D. T. Adroja and Myung-Hwan Whangbo, Inorg. Chem., DOI: 10.1021/ic201023j (2011)
- [23] P.A. Lindgård, A. Kowalska and P.Laut, J phys.Chem.Sol., **37**, 1357 (1967).
- [24] J. des Cloizeaux and J.J. Pearson, Phys. Rev. **128**, 2131 (1962).
- [25] N.G. Parkinson et al, J. Mater, Chem. **13**, 1468 (2003).
- [26] T. Chatterji, L. P. Regnault, P. Thalmeier, R. van de Kamp, W.Schmidt, A. Hiess, P. Vorderwisch, R. Suryanarayanan, G. Dhalenne, and A. Revcolevschi, J. Alloys Compd. **326**, 15 (2001).
- [27] T.G. Perring, D.T. Adroja, G. Chaboussant, G. Aeppli, T. Kimura and Y. Tokura, Phys. Rev. Lett. **87**, 217201 (2001).

- [28] S.M. Rezende and R.M. White, Phys. Rev. B **18**, 2346 (1978).
- [29] G. Xu , C. Broholm, D. H. Reich and M. A. Adams, Phys. Rev. Lett. **84**, 4465 (2000).
- [30] A.B. Harris et al, Phys. Rev. B **3**, 961 (1971).
- [31] R.J. Birgeneau, H.J. Guggenheim and G. Shirane, Phys. Rev. B **1**, 2211 (1970).
- [32] C.M.J. van Uijen, E. Frikkee and H.W. de Wijnl, Phys. Rev. B **19**, 509 (1979).
- [33] P. Hohenberg and W. Kohn, Phys. Rev. **136**, 864 (1964); M.H. Whangbo, H.-J. Koo, D.J. Dai, Solid State Chem. **176**, 417 (2003).
- [34] G. Kresse and J. Hafner, Phys. Rev. B **47**, 558 (1993).
- [35] G. Kresse and J. Furthmüller, Comput. Mater. Sci, **6**, 15 (1996)
- [36] G. Kresse and J. Furthmüller, Phys. Rev. B **54**, 11169 (1996).
- [37] J.P. Perdew, K. Burke and M. Ernzerhof, Phys. Rev. Lett. **77**, 3865 (1996).
- [38] S.L. Dudarev, G. A. Botton, S.Y. Savrasov, C.J. Humphreys and A.P. Sutton, Phys. Rev. B **57**, 1505 (1998).
- [39] K.A. Regan, Q. Huang and R.J. Cava. J. Solid State Chem. **178**, 2014 (2005); J. T. Haraldsen, M. B. Stone, M. D. Lumsden, T. Barnes, R. Jin, J. W. Taylor, and F. Fernandez-Alonso, J.Phys. Cond. Matter **21**, 506003 (2009).

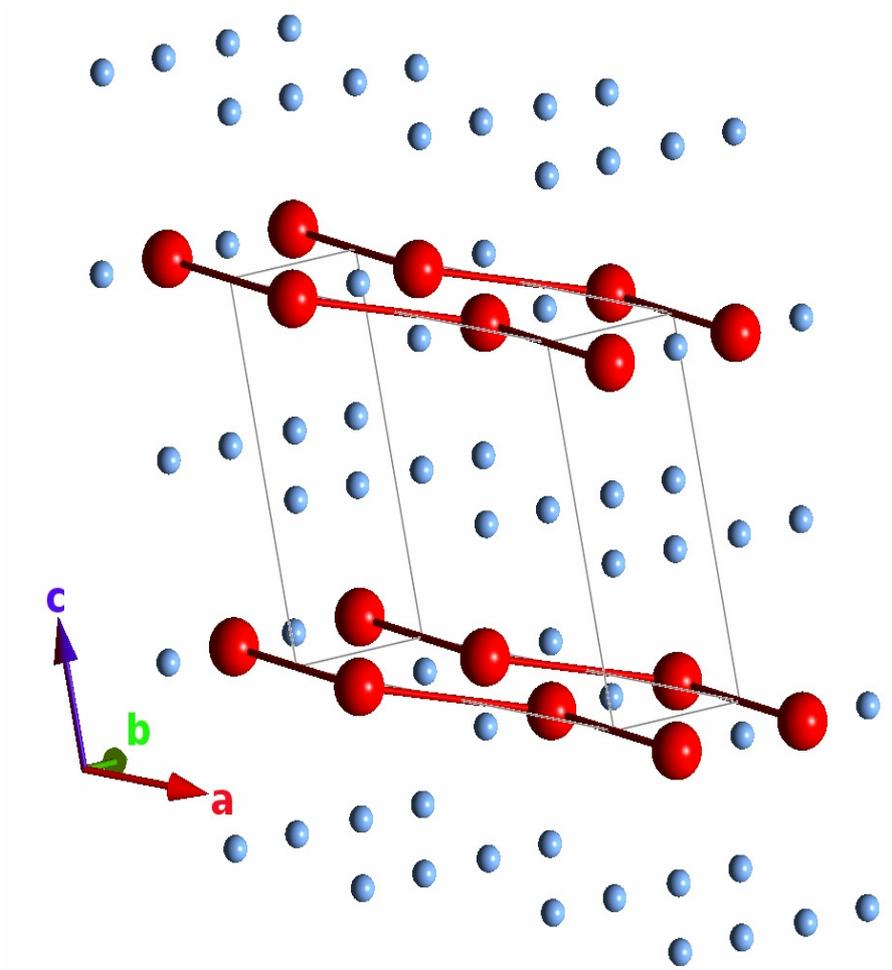


**Fig.1a P. Manuel et al**

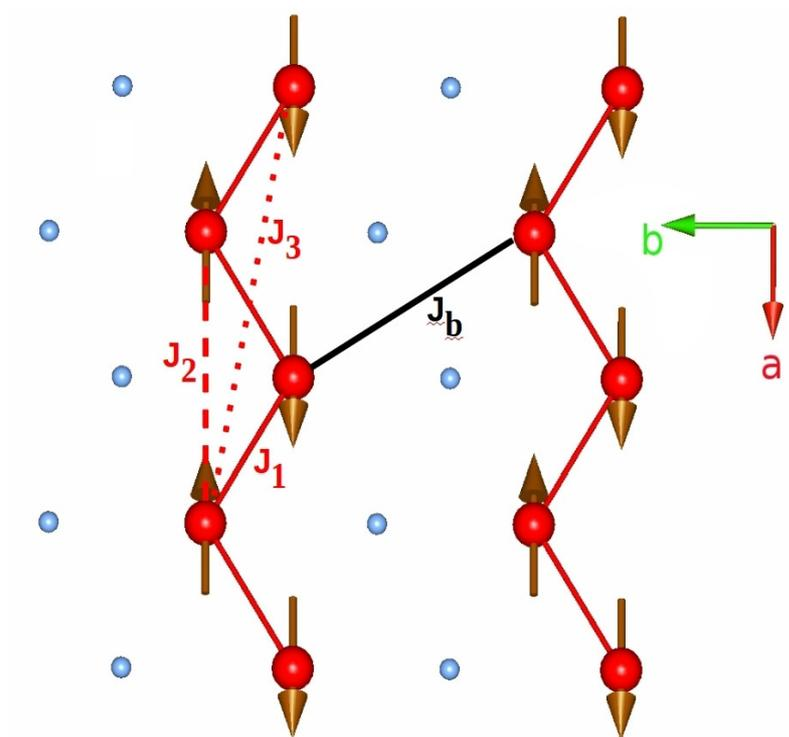


**Fig.1b P. Manuel et al**

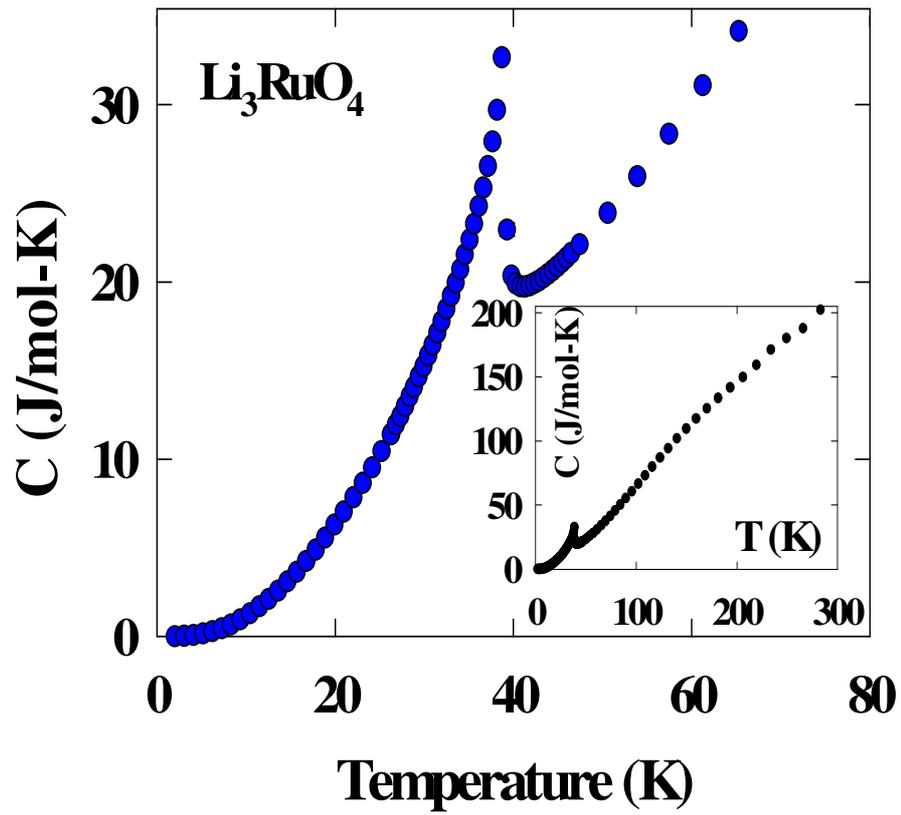


**Fig. 2 P. Manuel et al**

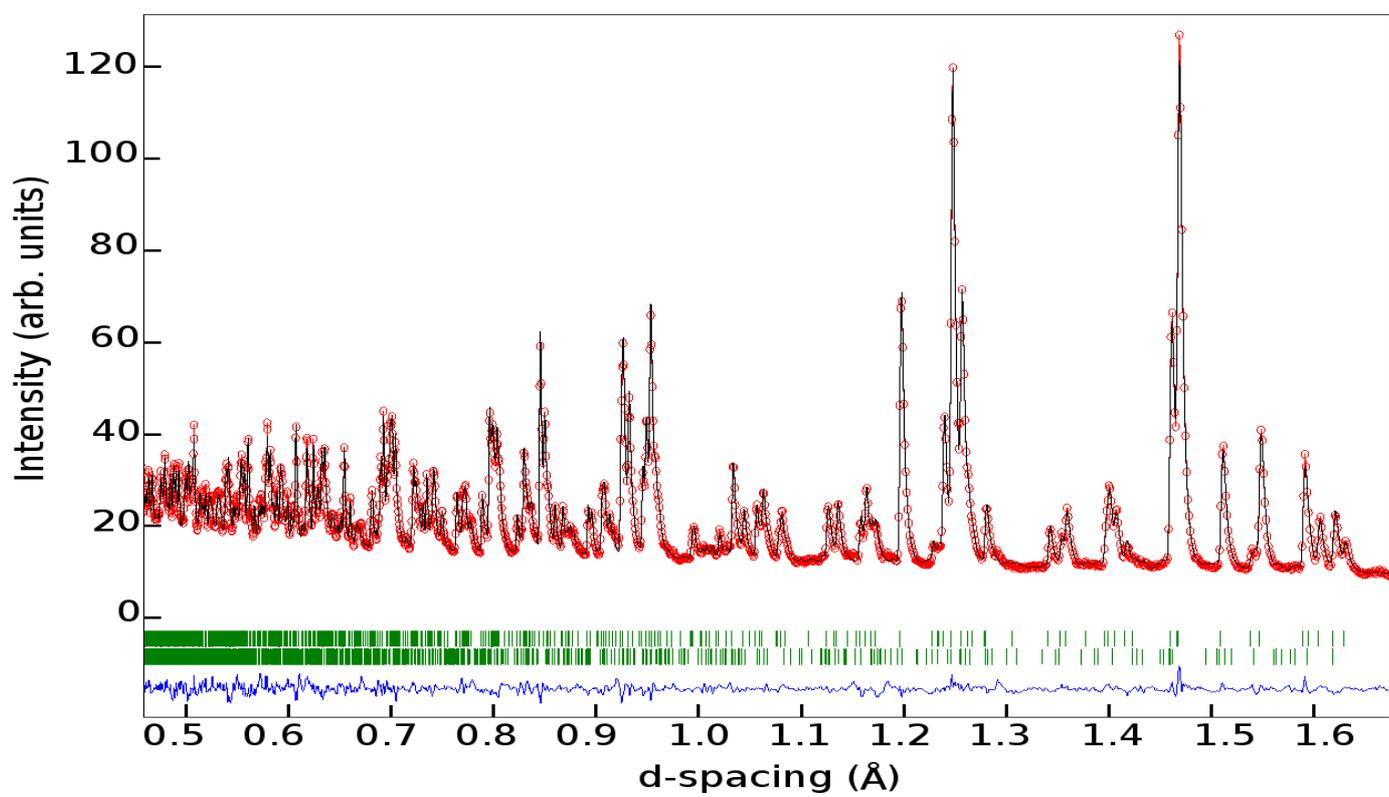


**Fig. 3 P. Manuel et al**

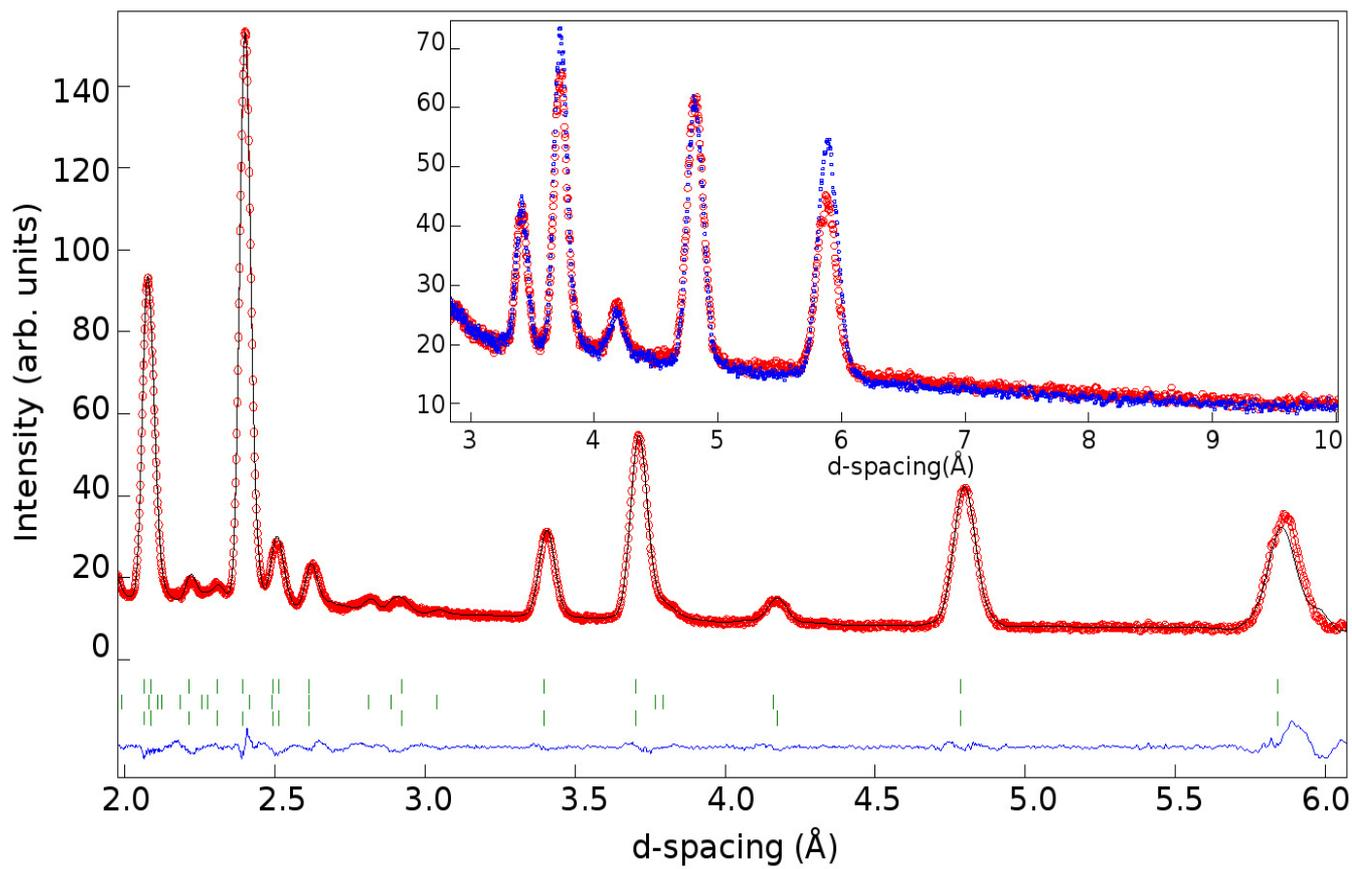


**Fig. 4 P. Manuel et al**

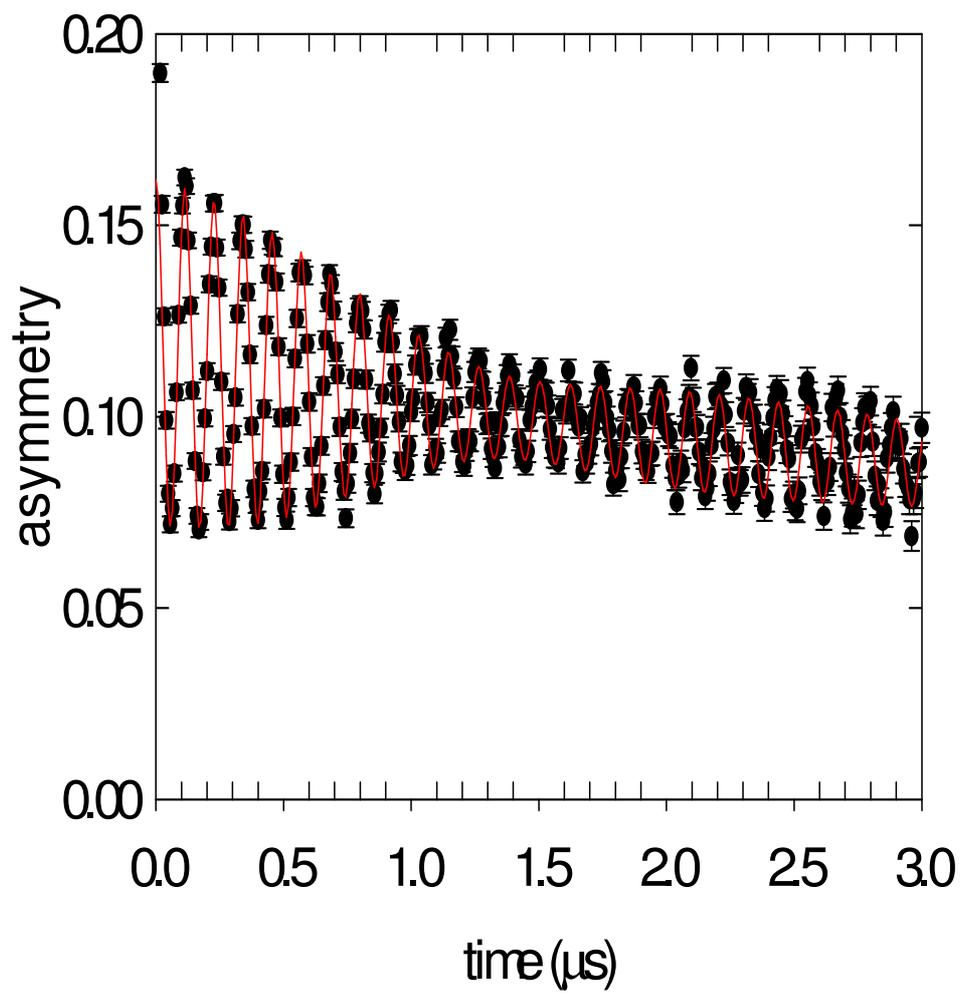


**Fig. 5 P. Manuel et al**

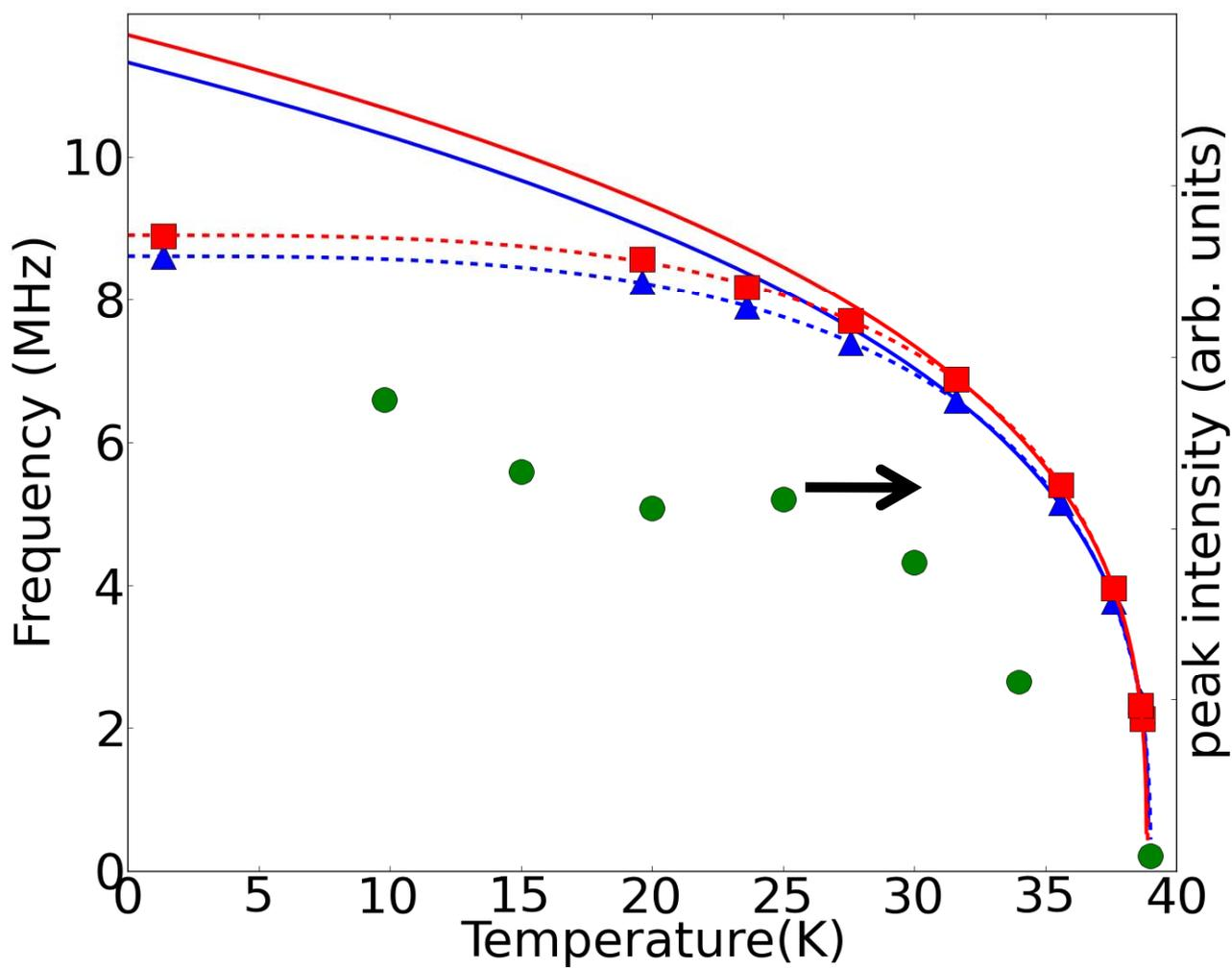


**Fig. 6 P. Manuel et al**

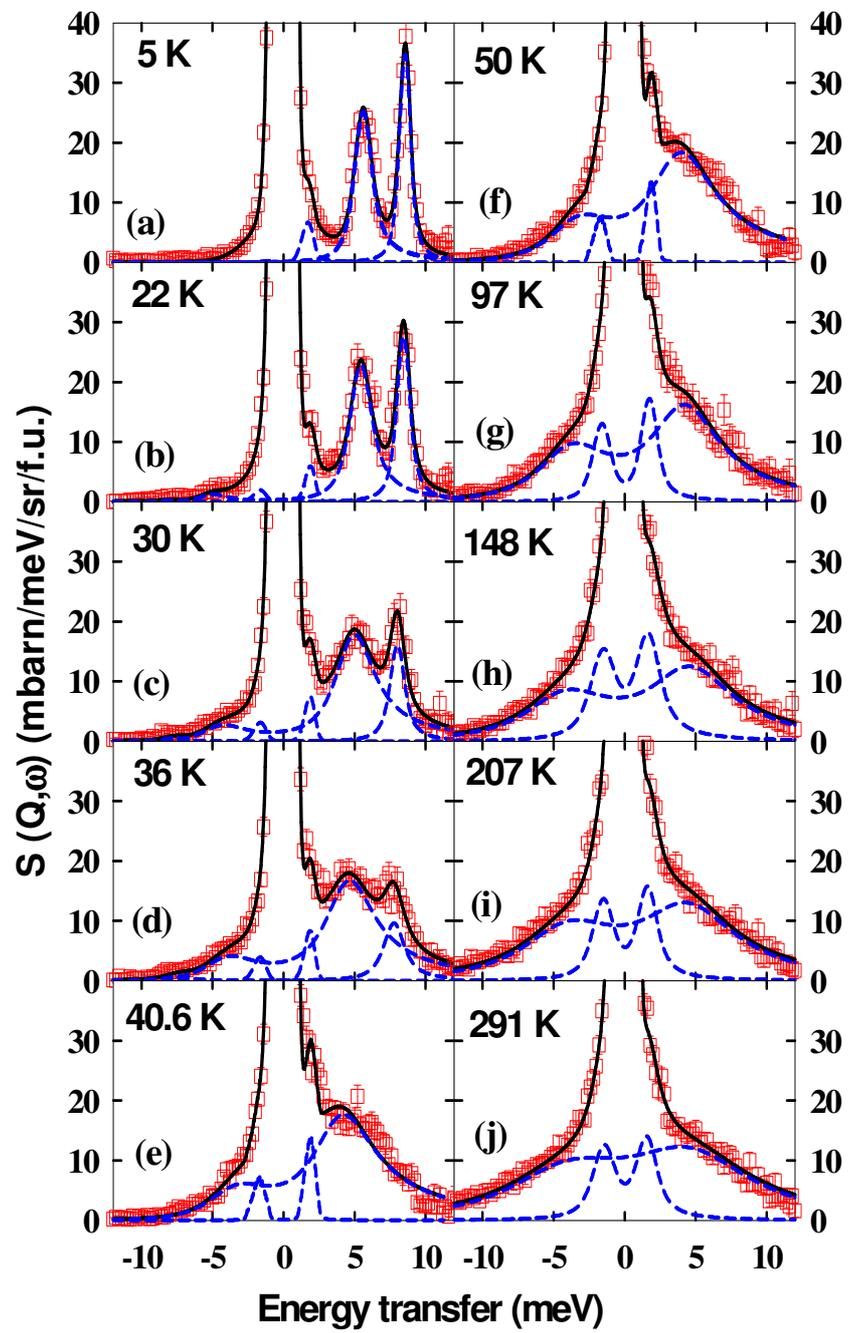


Fig.7 P. Manuel et al

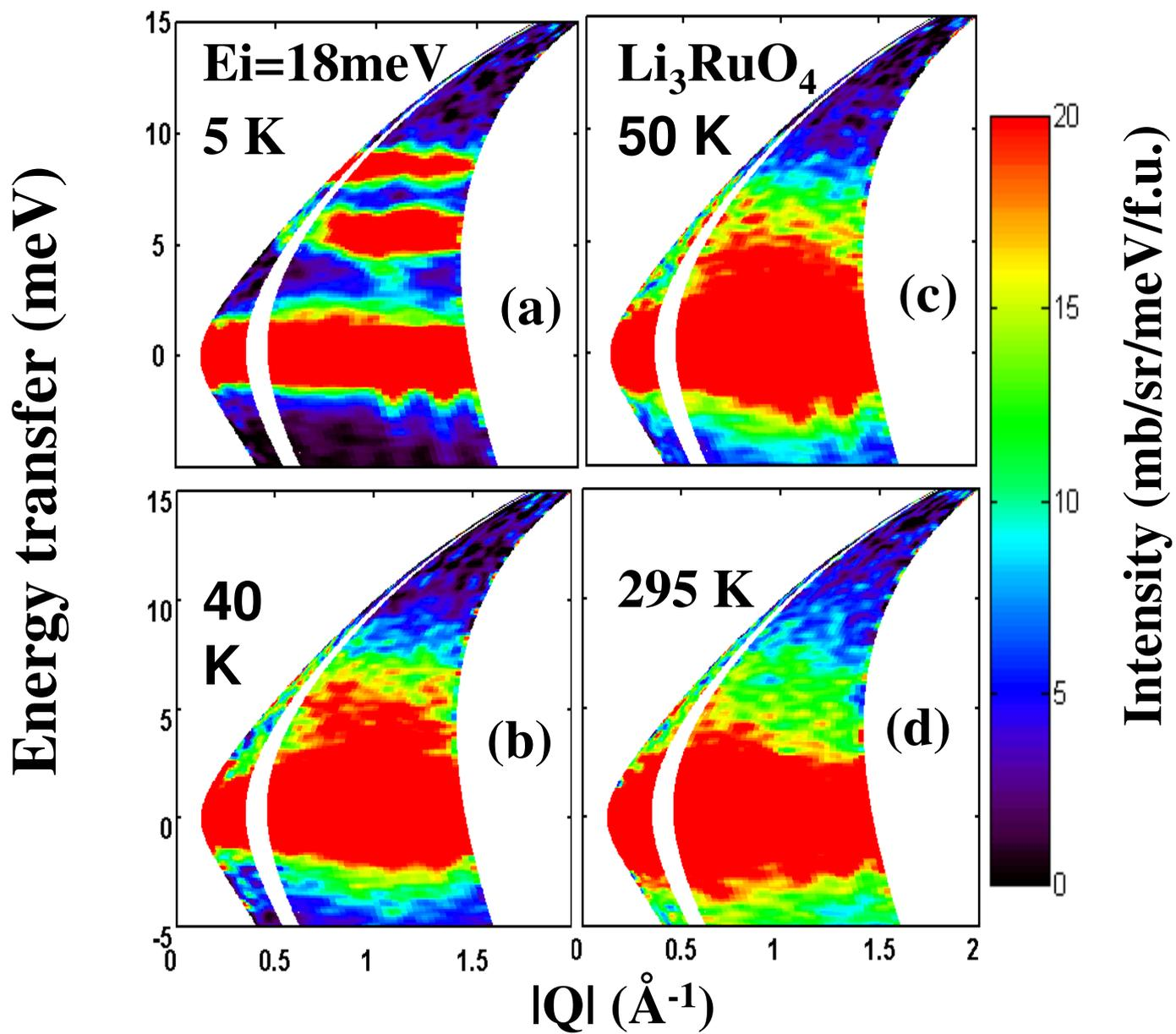


Fig.8 (a-d) P. Manuel et al

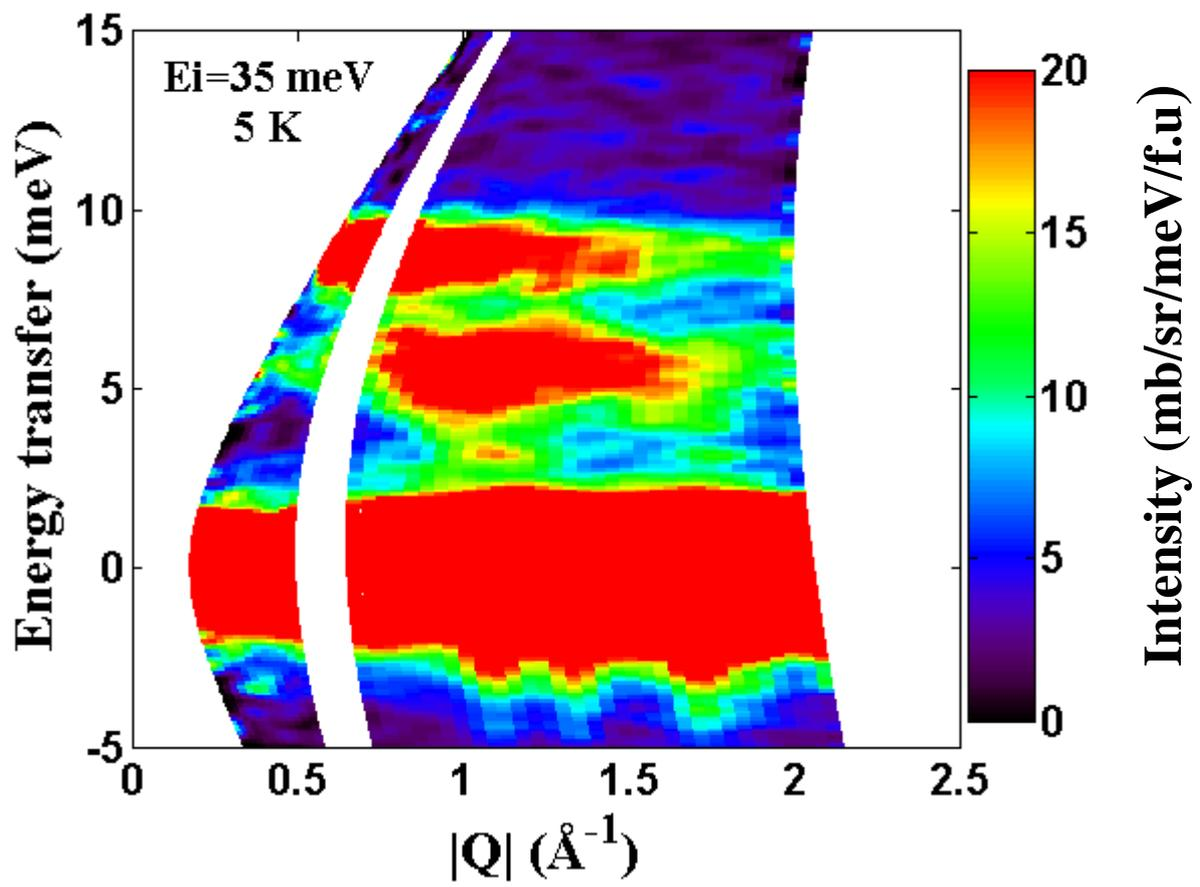


Fig. 9 P. Manuel et al

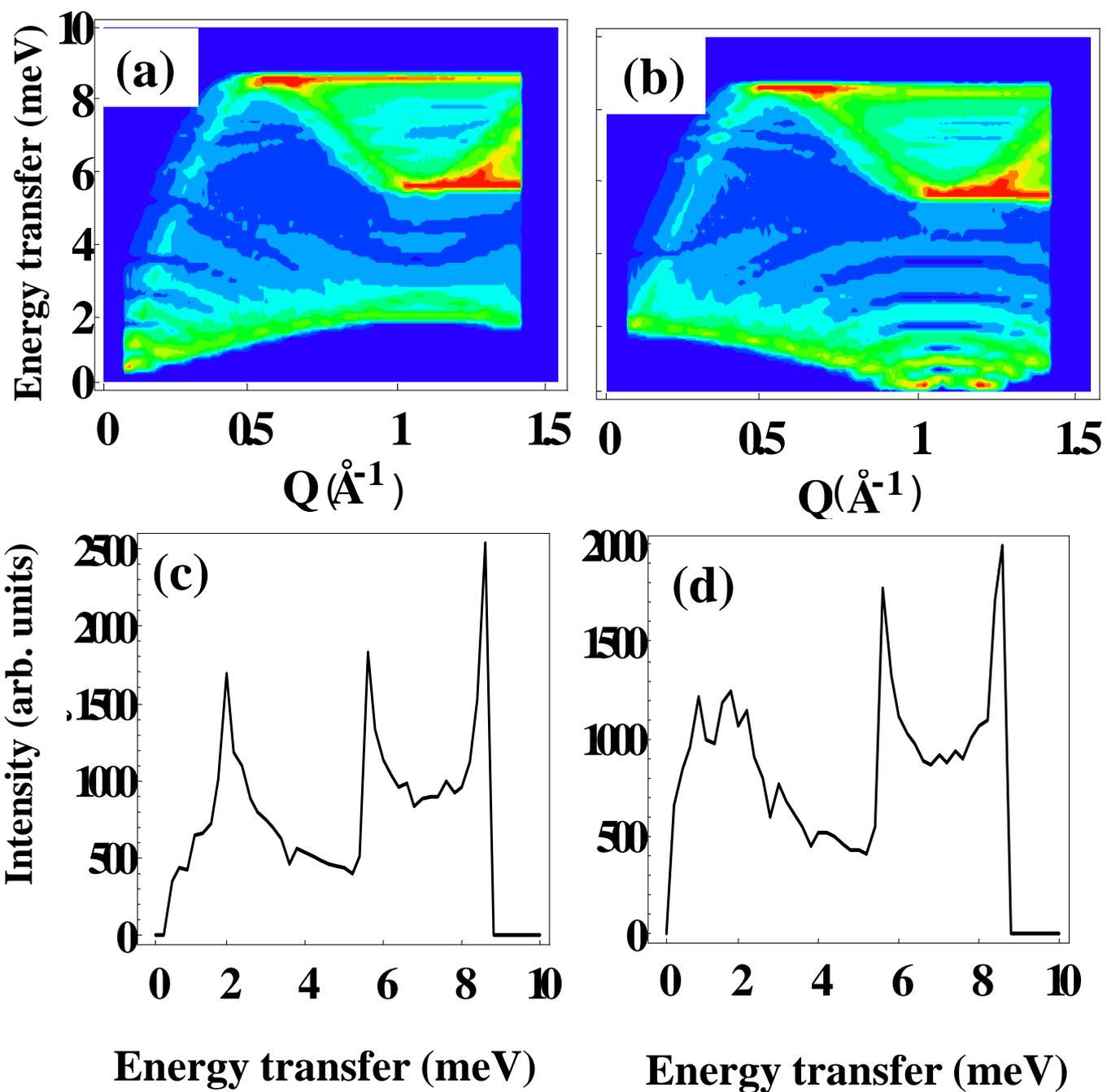


Fig.10 (a-d) P. Manuel et al

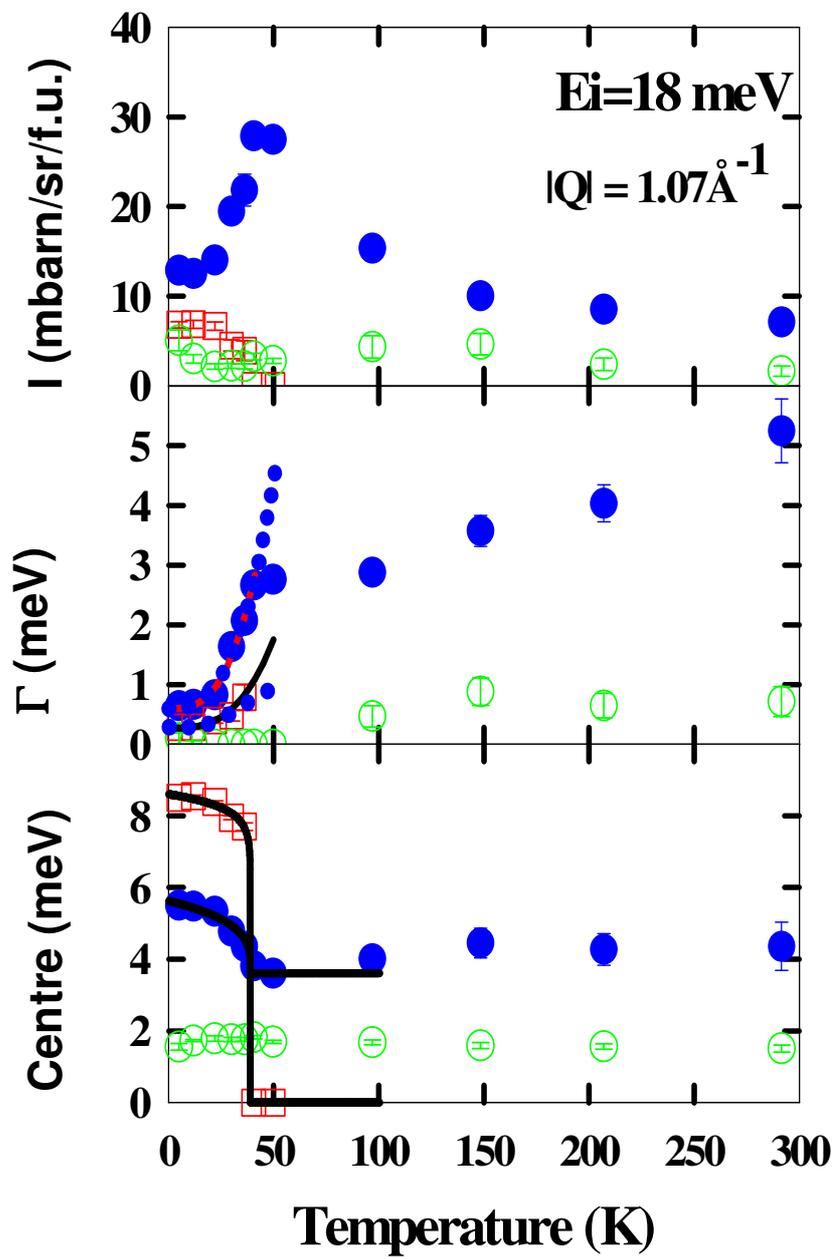


Fig. 11 P. Manuel et al

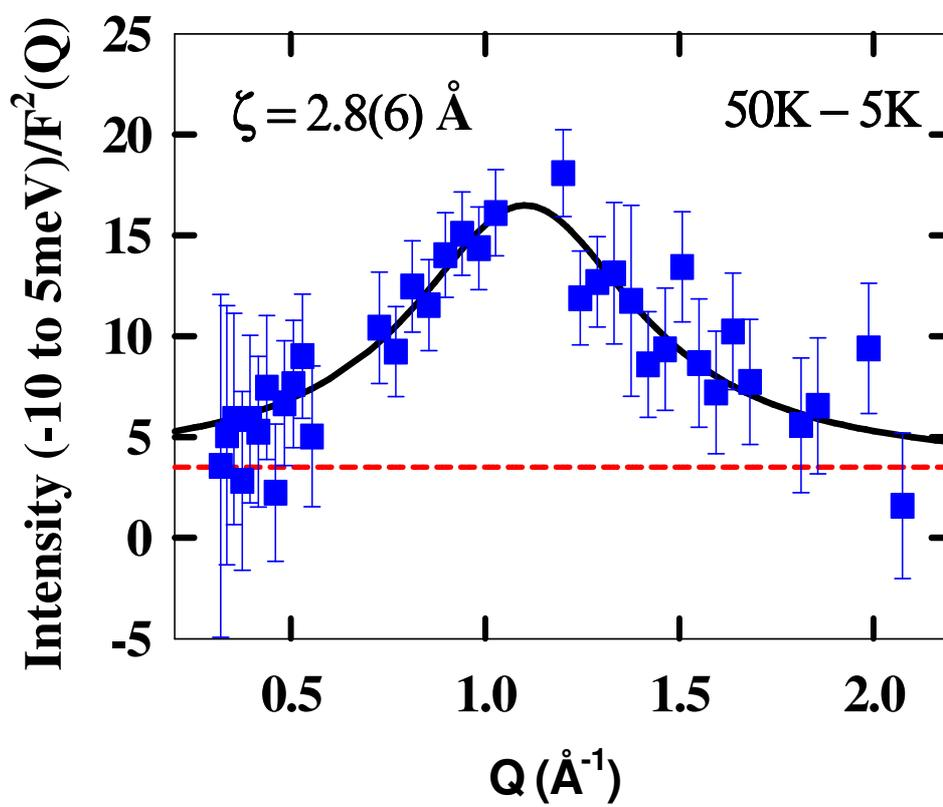


Fig.12 P. Manuel et al